IEEE Photonics Journal
An IEEE Photonics Society Publication

Open Access

Quasi-Phase-Matched Faraday Rotation in Semiconductor Waveguides With a Magnetooptic Cladding for Monolithically Integrated Optical Isolators

Volume 5, Number 6, December 2013

David C. Hutchings, Senior Member, IEEE
Barry M. Holmes, Member, IEEE
Cui Zhang
Prabesh Dulal
Andrew D. Block
Sang-Yeob Sung
Nicholas C. A. Seaton
Bethanie J. H. Stadler, Senior Member, IEEE

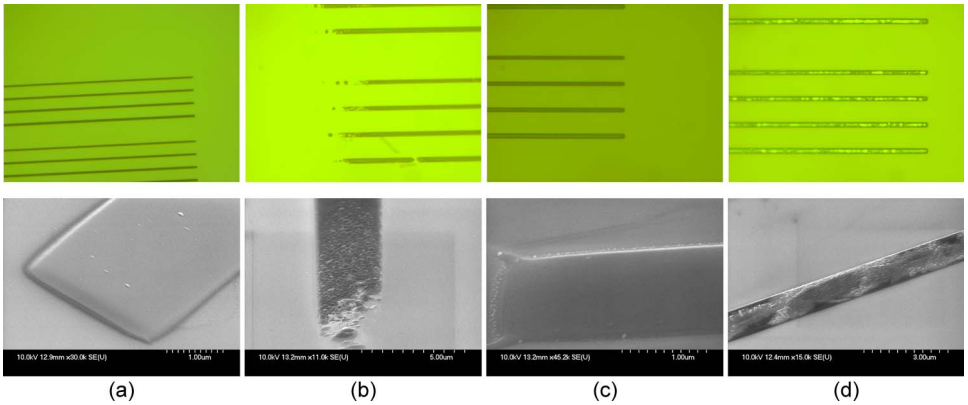

(a) (b) (c) (d)

DOI: 10.1109/JPHOT.2013.2292339
1943-0655

IEEE photonics SOCIETY

IEEE

Quasi-Phase-Matched Faraday Rotation in Semiconductor Waveguides With a Magnetooptic Cladding for Monolithically Integrated Optical Isolators

David C. Hutchings,[1] *Senior Member, IEEE*, Barry M. Holmes,[1] *Member, IEEE*, Cui Zhang,[1] Prabesh Dulal,[2] Andrew D. Block,[3] Sang-Yeob Sung,[3] Nicholas C. A. Seaton,[4] and Bethanie J. H. Stadler,[2,3] *Senior Member, IEEE*

[1]School of Engineering, University of Glasgow, Glasgow, G12 8QQ, U.K.
[2]Department of Chemical Engineering and Materials Science, University of Minnesota, Minneapolis, MN 55455 USA
[3]Department of Electrical and Computer Engineering, University of Minnesota, Minneapolis, MN 55455 USA
[4]Department of Earth Sciences, University of Minnesota, Minneapolis, MN 55455 USA

DOI: 10.1109/JPHOT.2013.2292339

Manuscript received October 16, 2013; revised November 6, 2013; accepted November 7, 2013. Date of publication November 21, 2013; date of current version December 4, 2013. This work was supported as a World Materials Network in part by the Engineering and Physical Sciences Research Council under Grant EP/J018708/1 and in part by the National Science Foundation under Grant DMR-1210818.
Corresponding author: D. C. Hutchings (e-mail: David.Hutchings@glasgow.ac.uk).

Abstract: Strategies are developed for obtaining nonreciprocal polarization mode conversion, also known as Faraday rotation, in waveguides in a format consistent with silicon-on-insulator or III–V semiconductor photonic integrated circuits. Fabrication techniques are developed using liftoff lithography and sputtering to obtain garnet segments as upper claddings, which have an evanescent wave interaction with the guided light. A mode solver approach is used to determine the modal Stokes parameters for such structures, and design considerations indicate that quasi-phase-matched Faraday rotation for optical isolator applications could be obtained with devices on the millimeter length scale.

Index Terms: Magnetophotonics, waveguide devices, integrated photonic systems.

1. Introduction

The nonreciprocal optical effect of Faraday rotation is widely exploited in optical isolators to suppress back-reflections to protect optical sources and other devices from injection noise, or in optical circulators to route counter-propagating signals in a single physical channel to different ports. To date, these devices are assembled from bulk components. For example, an optical isolator normally consists of two linear polarizers set at 45° to each other, a bulk or normal-incidence thin film magnetooptic crystal (usually from the iron garnet family) and a permanent magnet. The consequence of using bulk components to build optical systems is that the assembly and alignment of the components limits production volumes, affects reproducibility and yield, and becomes a major part of the overall manufacturing cost. Conversely, photonic integration has proved technically successful in developing techniques for combining multiple optical devices onto a single chip with the benefits of added

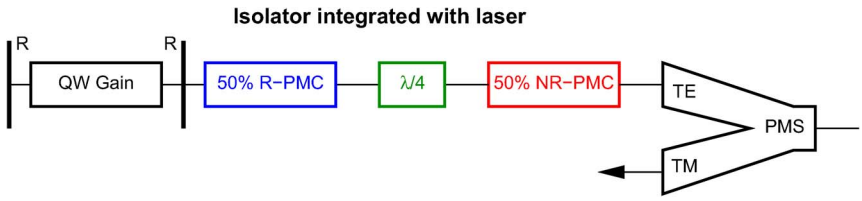

Fig. 1. Building blocks for integrated waveguide devices. The nonreciprocal polarization mode converter section is shown in red, the universal 3 dB reciprocal polarization mode converter section is shown in blue, and a fixed differential phase retarder is shown in green. Additional polarization discrimination may be provided by polarization mode splitters (PMS) and anisotropic gain in a quantum well laser.

functionality, and reduction in costs, arising from the replacement of manual assembly and alignment of individual components with lithographic techniques.

2. Background

There are a number of challenges to be overcome in the implementation of magnetooptic elements in optoelectronic integrated circuits (OEIC) or photonic integrated circuits (PIC) [1]. At near-IR wavelengths the iron garnets are overwhelmingly best suited as magnetooptic materials due to the comparatively large imaginary off-diagonal terms in the dielectric tensor while retaining a low optical loss. The first challenge is a consequence of the typical refractive indices for garnets being far smaller than the guiding layer in semiconductor OEIC/PICs. Butt-coupling of such heterogeneous materials, which would be technologically challenging anyway, will result in interface (Fresnel and mode-mismatch) reflections, which are obviously undesirable in an optical isolator. An alternative configuration, which is becoming widely deployed in integrated magnetooptics, is to use the evanescent interaction with a magnetooptic medium as an upper cladding to a semiconductor guiding layer [1], [2]. This cladding approach has also been used with the nonreciprocal phase-shift obtained through the transverse magnetooptic Kerr effect with direct bonding [3], [4], adhesive bonding [5], [6] and deposition [7] on silicon-on-insulator wafers.

The second challenge to the facilitation of optical isolation by Faraday rotation in an integrated format is that, while there are solutions to provide polarizers, or polarization mode splitting, with a polarization orientation in-plane or normal to the wafer, it is not straightforward to do this for an arbitrary (in this case 45°) orientation. One solution to this is to incorporate a reciprocal polarization mode converter (R-PMC), which has the functionality of a birefringent waveplate, based on an asymmetric profile waveguide [6], [8]–[12]. The required reciprocal polarization mode conversion can be achieved either with a quarter-waveplate with optic axis at 45° or a half-waveplate with an optic axis at 22.5° equivalents. The physical realization of an effective optic axis at 45° in a guided wave format can only be approached asymptotically and therefore the half-waveplate with an effective optic axis at 22.5° offers a more practical solution [13].

Fig. 1 shows a schematic of a possible implementation of an integrated optical isolator based on Faraday rotation. The final polarization mode splitter (PMS) is only necessary should there be significant TM-polarized reflected light in the system. The quantum-well laser provides the other polarization discrimination as it emits TE-polarized light from the heavy-hole transition, yet is transparent to TM-polarized light at the lasing wavelength. The combination of a nonreciprocal polarization mode converter and a reciprocal polarization mode conversion cancel each other in the forward direction, but provide a cumulative TE- to TM-polarization mode conversion in the reverse. The additional quarter-waveplate ensures the correct phase between the polarization modes with the half-waveplate R-PMC design.

The third challenge to be able to exploit Faraday rotation in an integrated format is a consequence of the planar format of OEIC/PICs which introduces a birefringence into the waveguides, and will form the principal subject for this paper. Faraday rotation is an example of coherent mode-conversion where the direction of energy transfer is phase dependent. A mismatch in modal phase velocities places a constraint on the extent of the energy transfer between modes.

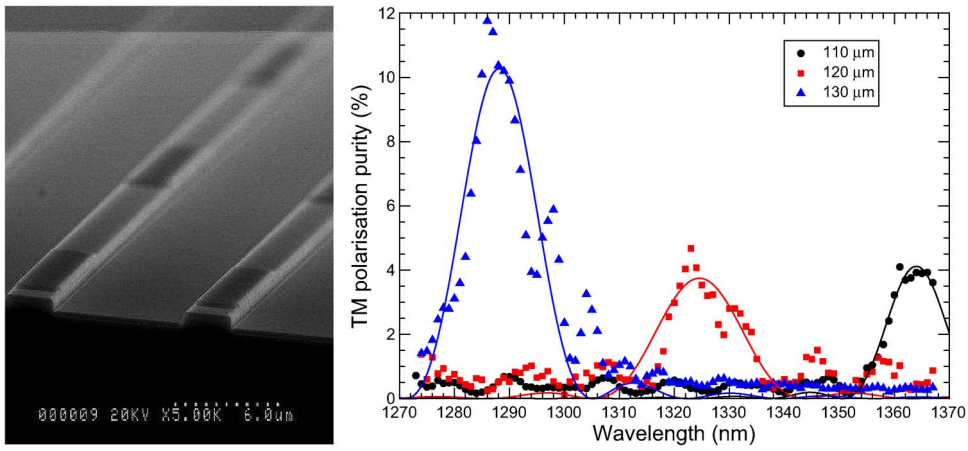

Fig. 2. GaAs waveguides with alternating upper cladding between magnetooptic material and silica (left). Fraction of TM-polarized output from a TE-polarized input due to nonreciprocal polarization mode conversion under remanent magnetization (right). From Ref. [21].

This phase-matching requirement was first recognized in optics for optical frequency generation. Quasi-phase-matching (QPM) is a technique where the medium is spatially modified periodically to compensate for a phase velocity mismatch and ensure a monotonic flow of energy between the modes. The most widely exploited QPM technique is domain reversal [14] achieved by stacking plates, by dopant diffusion, by electric-field poling, or by growth on orientation-patterned substrates. More generally, the extent of the monotonic modal conversion is determined by magnitude of the appropriate order (normally first-order) spatial Fourier coefficient [15]. Hence, frequency conversion has also been demonstrated by modulating the magnitude of the nonlinear coefficient, for example by spatially patterned quantum-well intermixing of superlattice waveguides [16], [17].

Quasi-phase-matching can also be applied to nonreciprocal polarization mode conversion. Initial demonstrations were on a planar waveguide format with mode confinement in the vertical direction only. Tien *et al.* used a serpentine current strip to provide a periodically reversed applied magnetic field [18]. Wolfe *et al.* used post-deposition laser annealing to modify a (Bi, Ga) YIG film, with a composition close to the compensation point, providing a change in the sign of the net magnetooptic coefficient [19]. A similar approach was used by Ando *et al.* who used post-deposition laser annealing to change the direction of the magnetization vector [20].

3. First Demonstration of QPM Faraday Rotation in a Rib Waveguide

An implementation of nonreciprocal mode conversion suitable for an OEIC/PIC requires a compatible core medium and both horizontal and vertical optical confinement in a rib or channel waveguide. This was achieved in a 2.7 μm wide and 0.5 μm thick GaAs rib waveguide with an $Al_{0.27}Ga_{0.73}As$ lower cladding and a periodically structured upper cladding [21]. Segments of non-magnetooptic dielectric (silica or silicon nitride) were fabricated by reactive-ion etching, or lift-off on top of the GaAs rib. The entire sample was coated with a film obtained by sputtering a CeYFeO target (achieving $Ce_1Y_2Fe_5O_x$ stoichiometry measured using energy dispersive X-ray techniques), as shown in Fig. 2 (left). The deposited film was not annealed and therefore was not crystalline, but it did exhibit ferromagnetism with a measured coercivity of 40 Oe.

The samples were magnetically saturated by applying a magnetic field parallel to the waveguides. A tunable laser was used to launch TE-polarized light into 8 mm long waveguides. The measured range of optical losses were 0.9 dB/mm at 1367 nm to 1.2 dB/mm at 1287 nm. The transmitted polarization state was analyzed as affected solely by the remanent magnetization. Fig. 2 (right) shows the measured fraction of TM-polarized transmitted light. The curves are best fits of $(\sin x/x)^2$ to the measured data, which is the usual dependency for phase-matching conversion efficiency. It can be seen that there is an enhancement of the modal conversion around a particular

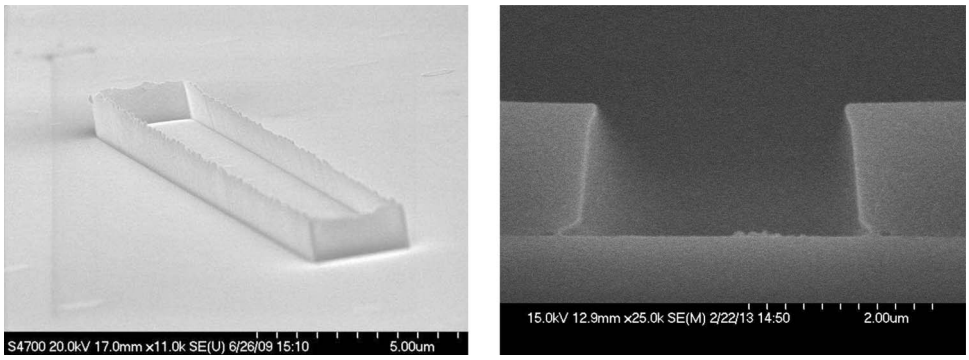

Fig. 3. Result of garnet precursor deposition and lift-off with a single layer PMMA mask, with the sidewall deposition producing an open top box shape (left). Cross-section of bi-layer PMMA mask (with overhang) for lift-off on GaAs wafer prior to garnet precursor deposition (right).

wavelength, which varies with the QPM period due to dispersion. The measured maximum of 12% TM-polarized component at 1287 nm was confirmed to be nonreciprocal by determining the orientation of a polarizer which minimized the transmission, which was found to be its mirror image with either reversing the saturating magnetic field, or turning the sample around without modifying the remanent magnetization.

The waveguides in this demonstration supported both fundamental and first-order waveguide modes. On calculating the supported modes and their effective indices, it was found that the QPM periods corresponded to coupling the first-order TE-polarized mode to the fundamental TM-polarized mode. Therefore, with the majority of the coupled input launched into the fundamental TE-polarized mode, the measured polarization conversion of up to 12% corresponds to a large fraction of the power in the available mode.

Subsequent attempts were made to crystallize the magnetooptic upper cladding using a rapid temperature anneal (RTA). However, it was found that the mismatch in thermal expansion between this film and the underlying sample caused catastrophic mechanical failure and delamination of the film.

4. Segmented Cladding Fabrication Development

The mismatch in thermal expansion between garnets and semiconductor substrates can be accommodated by restricting the precursor deposition to sufficiently small segments, such as the micron scale width of optical waveguide cores or claddings, prior to crystallization under annealing [22]. Phosphoric acid etch has been shown to define garnet waveguides on silica. However, this wet etching results in non-vertical sidewalls and, more importantly, it is incompatible with III-V wafers which it etches at a faster rate than the garnet precursor.

Consequently, a lift-off process has been developed in order to pattern the deposited amorphous garnet precursor using a PMMA resist mask written using e-beam lithography. The initial attempts at this used a single layer of PMMA, but the conformal coating normally experienced in sputtering system leads to significant side-wall deposition as shown in Fig. 3 (left). Therefore, a bi-layer PMMA resist mask was employed, consisting of a 15% dilution (1.2 μm thick) lower layer, with a molecular weight of 2010, and a 4% dilution (0.2 μm thick) upper layer, with a molecular weight of 2041. The higher molecular weight of the upper layer results in a slightly thinner opening at the top of the mask, leading to an overhang profile as shown in Fig. 3 (right). Careful optimization of the e-beam writing parameters results in both the size of the desired features (in this case widths of between 200 nm and 2 μm with lengths from 10 μm to several millimeters), as well as the required overhanging sidewall profile of the mask, to be obtained reproducibly. The garnet precursor was deposited using RF sputtering with argon plasma with 20.4 sccm Ar flow. The Fe target was sputtered at 220 W while the Y (and Tb) targets were sputtered at 120 W. The deposition was performed with a 2.0 sccm oxygen flow and the chamber pressure was held at a constant 6.0 mtorr.

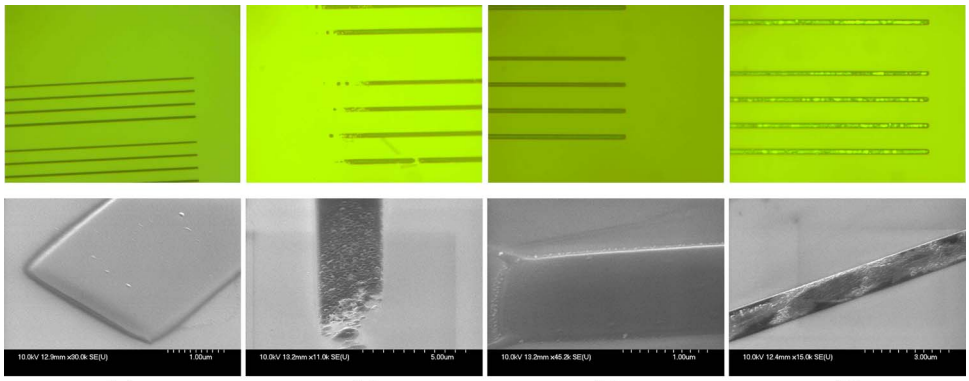

Fig. 4. Optical (upper) and scanning electron (lower) micrographs of garnet segments after lift-off with (a) precursor as deposited on SOI, (b) deposited on SOI, anneal at 800 °C, (e) deposited on MgO layer on SOI, anneal at 800 °C, and (d) deposited on MgO layer on SOI, anneal at 900 °C (see text).

For the deposition of garnet on silicon-on-insulator (SOI), the e-beam dose for the PMMA mask was ∼1000 μC/cm^2 and 120 nm of deposited material results in ∼85 nm thick segment in the examples shown here due to the restriction in atomic velocity angles by the lift-off mask (similar to the cause of the reactive-ion etch lag phenomenon [10]). Fig. 4 shows optical (top) and scanning electron (bottom) micrographs of the segmented YIG deposition on SOI after removal of the PMMA mask. Where a rapid thermal anneal is performed it is in 150 mB oxygen for 120 s. The micrographs correspond to (a) as-deposited, (b) direct deposition on SOI and anneal at 800 °C, (c) deposition on a 5 nm MgO layer, which had been first deposited on the SOI wafer, and anneal at 800 °C, and (d) deposition on 5 nm MgO layer on SOI and anneal at 900 °C. It can be seen that sidewall deposition has been inhibited with the bi-layer mask, with smooth edges to the segments. Some erosion of the deposited segment when deposited directly on the silicon surface is observed upon annealing under these conditions. This problem was avoided by annealing under flowing oxygen (10 slpm) at 850 °C for 120 s, or by first depositing a ∼5 nm layer of MgO on the silicon surface. The uniform morphology obtained at anneal temperatures of 800–850 °C are comparable to the YIG waveguides on SiO_2 formed by wet-etch, which had measured optical losses of ∼1 dB/mm at a wavelength of 1.55 μm [22]. Obvious changes to the segment morphology are visible for both optical and SEM at a higher temperature (900 °C) anneal, which we attribute to a larger grain size.

Information about the crystal structure of the segments following anneal was obtained using electron backscatter diffraction (EBSD). The diffraction pattern in the case of direct deposition on SOI and anneal at 800 °C was consistent across various positions on the sample and matched well with the reference YIG pattern from the database. This is consistent with isotropic polycrystalline YIG, with the small grain size not apparent in the SEM. In the case of the deposition on 5 nm MgO layer on SOI and anneal at 800 °C, there was some positional variation in the diffraction pattern, which nevertheless did provide a good match to the reference YIG pattern from the database in some areas. The positional variation may not necessarily be an indication of the existence of multiple phases of YFeO and could be due to the contribution to diffraction from the MgO layer. For the deposition on 5 nm MgO layer on SOI and anneal at 900 °C the diffraction pattern again had a spatial variation, but also was less well defined (which may be an indication of the presence of multiple phases or may be due to the influence of the larger grain size).

Fig. 5 shows an optical micrograph with a wider view of the SOI sample after anneal (the scale bar is 250 μm). The garnet precursor segments are 500 nm wide, and the segment and gap lengths range around the anticipated half-beat-lengths (see below). The segments are aligned so they will provide the magnetooptic component of the alternating upper cladding for QPM Faraday rotation.

For the deposition of garnet on the III-V wafer consisting of a GaAs guiding layer on AlGaAs cladding, the e-beam dose for the PMMA mask was ∼600 μC/cm^2. With 120 nm of deposited material the thickness of the segment ranged from ∼67 nm for a 1.0 μm gap to 120 nm for $\geq$ 3 μm

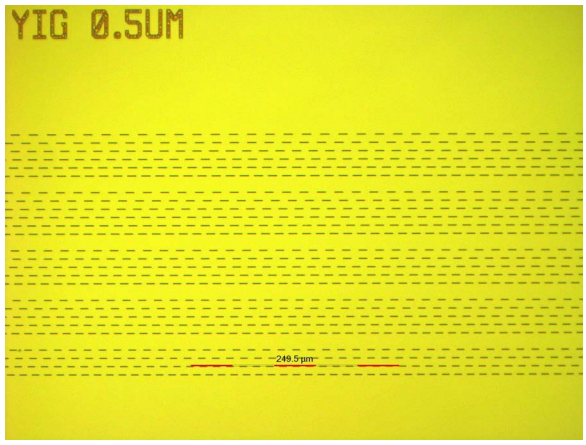

Fig. 5. Optical micrograph of fabricated YIG segments on SOI patterned to provide the alternating upper cladding for a QPM Faraday rotation waveguides. The segments are 500 nm wide and have a range of segment and gap lengths around the anticipated half-beat-lengths.

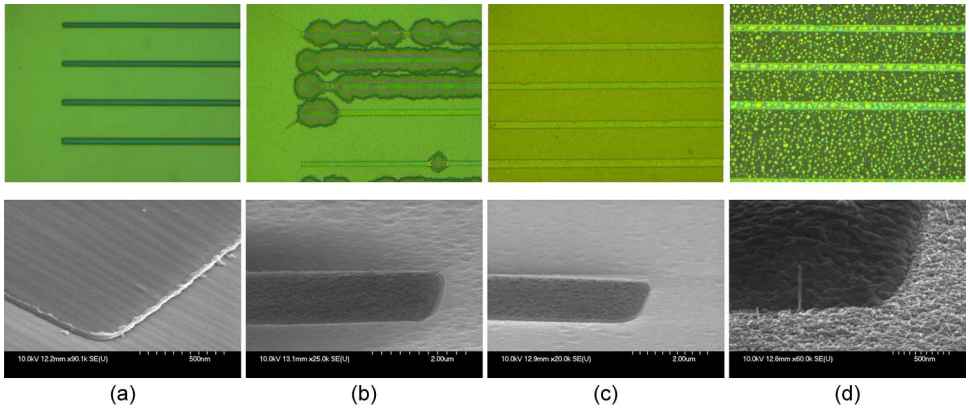

Fig. 6. Optical (upper) and scanning electron (lower) micrographs of garnet segments after lift-off with (a) precursor as deposited on GaAs, (b) deposited on GaAs, anneal at 700 °C, (c) deposited on MgO layer on GaAs, anneal at 700 °C, and (d) deposited on MgO layer on GaAs, anneal at 800 °C (see text).

gap. Fig. 6 shows optical (top) and scanning electron (bottom) micrographs of the segmented YIG deposition on GaAs guiding layer after removal of the PMMA mask. Where a rapid thermal anneal is performed it was also in 150 mB oxygen for 120 s. The micrographs correspond to (a) as-deposited, (b) direct deposition on GaAs and anneal at 700 °C, (c) deposition on 5 nm MgO layer on GaAs and anneal at 700 °C, and (d) deposition on 5 nm MgO layer on GaAs and anneal at 800 °C. It is found that there is a chemical reaction between the GaAs and the garnet precursor under RTA which results in the creation of voids at the interface. Consequently, in waveguiding structures the optical losses are found to drastically increase to the extent that there is no observed transmission of guided light. This detrimental chemical reaction can be avoided with the deposition of a 5 nm MgO layer. At the higher annealing temperature (800 °C), roughening of the GaAs surface over the whole sample is observed.

EBSD studies on these samples after 120 s anneal in oxygen at 700 °C showed no diffraction pattern for direct deposition on GaAs, and only hints of a diffraction pattern with the MgO layer, suggesting that the annealed YFeO is mainly in an amorphous state. For the 800 °C anneal with the MgO layer there was a diffraction pattern corresponding to YIG observed in some areas, but not across the entire sample, suggesting the YIG has partially crystallized. Further process optimization

at temperatures in the range 700–800 °C is required to seek a balance between YIG crystallization and GaAs surface roughening, possibly with the investigation of longer or repeated anneals.

The lift-off process has also been demonstrated to pattern segments of the precursors of cerium substituted YIG (Ce:YIG) and terbium iron garnet (TIG), both of which in their garnet form have larger and opposite sign for the saturated magnetooptic effect at room temperature in comparison to YIG.

5. Waveguide Simulation and Design

The following analysis will be restricted to waveguides that are conventionally termed *single-moded*, which is normally used to denote waveguides which support just two mutually orthogonally polarized, single-lobed guided modes. We will use the techniques presented in Ref. [13] where a mode solver incorporating the general tensor form for the dielectric constant [23] is used to determine the two optical modes of the waveguide element, and these are obtained in terms of the normalized Stokes parameters. Now, as these modes will be associated with propagation constants $\beta^{(1)}$ and $\beta^{(2)}$, respectively, the propagation evolution of a guided wave, that is a linear combination of the two modes, within an element will be oscillatory due to mode beating with a periodic length $2L_{1/2}$, where

$$L_{1/2} = \frac{\pi}{|\beta^{(1)} - \beta^{(2)}|} = \frac{\lambda}{2\left|n_{\mathbf{eff}}^{(1)} - n_{\mathbf{eff}}^{(2)}\right|}. \tag{1}$$

For the guided modes in single-moded rib and strip-loaded waveguides, the polarization state typically remains close to uniform over the transverse area that carries nearly all the power of the mode, and consequently it is useful to represent the modes with normalized, averaged values of the Stokes parameters

$$\overline{S}_j = \frac{\int\int S_j(x,y)\,\mathrm{d}x\,\mathrm{d}y}{\int\int S_0(x,y)\,\mathrm{d}x\,\mathrm{d}y} \qquad j = 1,2,3. \tag{2}$$

This allows the guided wave evolution to be represented by trajectories on a Poincaré sphere, in a similar manner to the plane waves for which it is normally applied. Hence, these mode-beating trajectories can be approximately represented by rotation about the axis that passes through the two modal points. The polarization state evolution for the proposed integrated optical isolator, as shown in Fig. 1, is shown schematically as a trajectory on the Poincaré sphere in Fig. 7, where the colors refer to (1) 3 dB reciprocal polarization mode conversion (blue), (2) a quarter-wave phase retardation (green), and (3) a sequence of quasi-phase-matched half-beat lengths of magnetooptic (red) and half-wave (non- magnetooptic) phase retarders (green) to provide a TE-polarized output.

Fig. 8 shows the calculated modulus of the Stokes parameters for the guided modes of a silicon-on-insulator waveguide with a 100 nm thick magnetooptic upper cladding, taken to have $n = 2.19$ (garnet) and $\varepsilon_{xy} = 0.17\mathrm{i}$ corresponding to a longitudinal magnetic field (parallel to the propagation direction). The magnitude of the magnetooptic effect has been exaggerated (about 20 times that for Ce:YIG), in order to make the effect on the contour plots apparent. The contour lines are at 3 dB intervals ranging from 0 (the peak value for the mode) to −45 dB. The peak value of $|S_2|$ is at least 20 dB below the peak value for $|S_1|$. The consequence of the Faraday rotation in the magnetooptic cladding is to modify the guided modes such that they now have a significant S_3 component. Upon reversing the direction of the applied magnetic field, the sign of the S_3 component changes. The averaged Stokes parameter vector for each of the two guided modes is rotated from the S_1 axis toward the S_3 axis: "TE-like" $\overline{\mathbf{S}} = (0.991, 0, -0.014)$ and "TM-like" $\overline{\mathbf{S}} = (-0.990, 0, 0.032)$ with effective indices $n_{\mathrm{eff}} = 3.1395$ and 3.0616, respectively, giving a half-beat length of 9.95 μm.

Table 1 shows the calculated characteristic parameters for a SOI waveguide (700 nm wide rib, 500 nm thick Si etched to 200 nm thickness as in Fig. 8) with various dielectric and magnetooptic (100 nm layer thick) upper claddings shown, with subsequent deposition of silica overcladding. In each half-beat-length segment (rotation of 180° around the modal axis) the trajectory on the

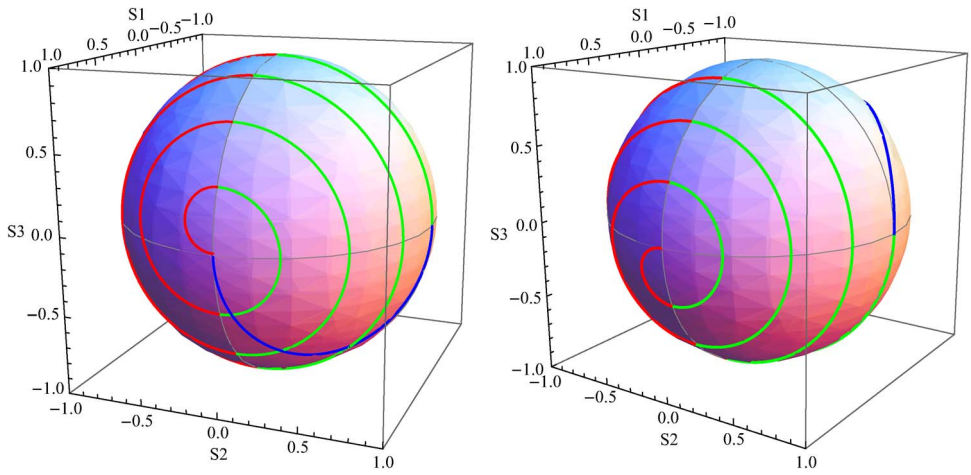

Fig. 7. Polarization state evolution shown as trajectories from a launched TE-polarized mode on the modified Poincaré sphere (see text) for forward (left) and backward (right) propagating light in the integrated optical isolator (from Ref. [13]).

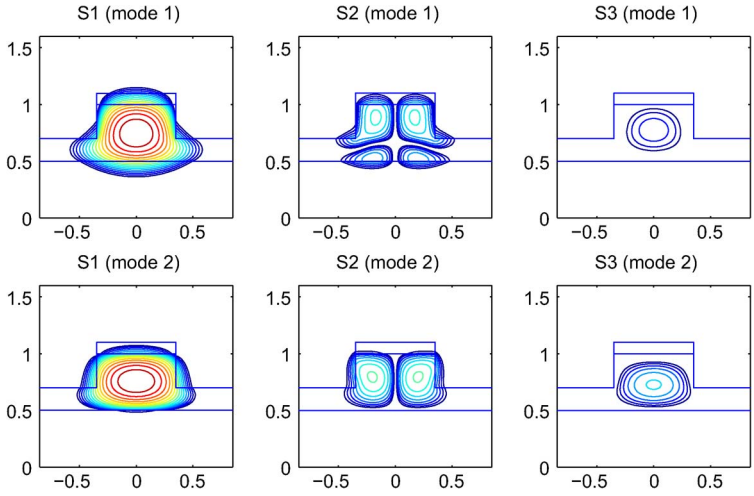

Fig. 8. The modulus of the Stokes parameters for the two guided modes at a wavelength of $\lambda = 1.55$ μm calculated using a full-vectorial mode solver. The horizontal and vertical scales are in μm. The 700 nm wide rib is composed of 500 nm thick Si (etched to 200 nm thickness) on a SiO_2 lower cladding with a 100 nm magnetooptic upper cladding.

Poincaré sphere changes the angle it makes with the S_1 axis by $2\sin^{-1}\overline{S}_3 \approx 2\overline{S}_3$ radians, where $\overline{S}_3$ is the average Stokes parameter corresponding to the relevant mode (see Fig. 7). As an example, take the QPM Faraday rotation where the upper cladding alternates between Ce:YIG and silica. The 50% conversion of a TE-polarized input will require $(\pi/2)/(2\overline{S}_3) = 1122$ periods. The length of each period is the sum of the two half-beat-lengths $9.95 + 8.05 = 18.00$ μm, giving a total NR-PMC length of 20.2 mm. The modulation in the magnetooptic effect can be enhanced by alternating garnet claddings with opposite signs. For example, taking a similar example using Ce:YIG and YIG claddings would require 1076 periods, but with a longer half-beat-length gives a total NR-PMC length of 21.1 mm. In the case of using alternating YIG and TIG claddings with these waveguide dimensions, the requirement is 6445 periods and a total NR-PMC length of 131.0 mm.

The garnets which are currently known to have the largest magnitude magnetooptic coefficients at optical communication wavelengths are cerium and bismuth substituted iron garnets.

TABLE 1

Coefficients used and calculated Faraday rotation parameters for a range of dielectric and magnetooptic garnet upper claddings on an SOI waveguide, as described in the text

	n	rotation (°/cm)	$\overline{S}_3/10^{-5}$ (TE)	$\overline{S}_3/10^{-5}$ (TM)	$L_{1/2}$ (μm)
SiO_2	1.44	0	0	0	8.05
5 nm MgO/SiO_2	1.44	0	0	0	8.10
100 nm YIG	2.1	200	3	-8	9.64
5 nm MgO/100 nm YIG	2.1	200	3	-2	9.51
100 nm TIG	2.3	-500	-9	18	10.38
5 nm MgO/100 nm TIG	2.3	-500	-8	5	10.10
100 nm Ce:YIG	2.19	-4500	-70	160	9.95
5 nm MgO/100 nm Ce:YIG	2.19	-4500	-64	44	9.77

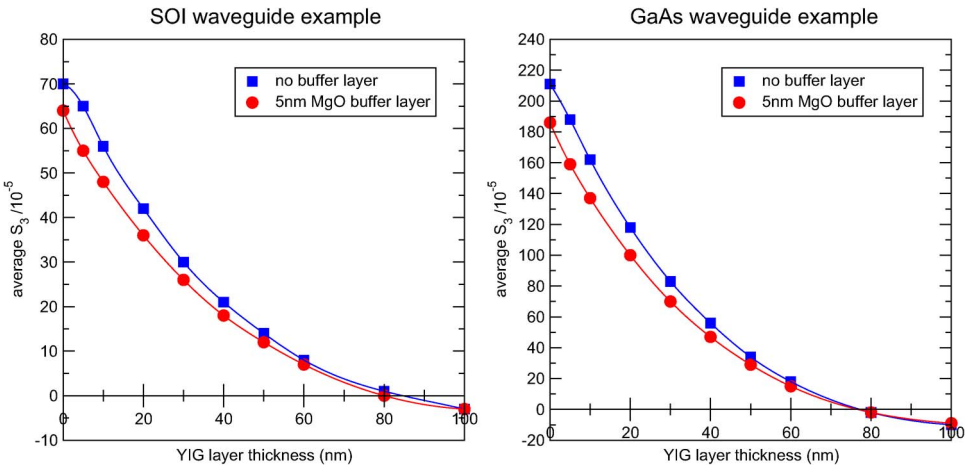

Fig. 9. Calculated average Stokes parameter $\overline{S}_3$ for the TE-like mode as a function of YIG seed layer thickness for Ce:YIG upper cladded waveguides (see text) based on silicon-on-insulator (left) and GaAs (right).

Unfortunately, these garnet species prove to be difficult to crystallize in a single phase by annealing when deposited on non-garnet substrates. However, YIG (and TIG) prove to be relatively straightforward to crystallize into a poly-crystalline form on silicon and many other non-garnet surfaces. By first depositing and annealing a YIG buffer layer, this can be used as a seed layer to subsequently deposit and anneal cerium-substituted [7] or bismuth [24] iron garnets and obtain the desired phase in polycrystalline form. It is observed that a minimum YIG layer thickness of ~20 nm is required in order to obtain polycrystalline Ce:YIG [7]. As the optical interaction is envisaged to be due to the evanescent wave in the garnet, the thickness of the seed layer will be important.

Fig. 9 shows the calculated average Stokes parameter $\overline{S}_3$ for the TE-like mode as a function of seed YIG layer thickness for the SOI waveguide example discussed earlier, and for a 0.6 μm thick and 1.1 μm GaAs waveguide on $Al_{0.6}Ga_{0.4}As$ lower cladding. The total garnet thickness was taken to be 100 nm, consisting of the YIG seed layer (200 °/cm) and Ce:YIG (-4500 °/cm). It can be seen that, due to the evanescent wave interaction into a cladding with a substantially lower index than the waveguide core, there is a steep reduction in the net magnetooptic effect which reduces to ~50% of the maximum value (without a seed layer) for just over 20 nm of YIG seed layer thickness. As a minimum seed layer thickness appears to be required in order to obtain crystallization of the substituted garnet, it is clear that some degree of compromise in the magnitude of interaction is inevitable. Note that modal overlaps with similarly compromised magnetooptic effects will also occur for the nonreciprocal phase shift method using deposited garnet claddings.

6. Conclusion

In this paper, a study of Faraday rotation in waveguides is undertaken, and the prospects for its incorporation into an integrated optical isolator, or circulator, are discussed. This paper concentrates on integration formats that are compatible with current photonic integrated circuit technologies, and in particular the use of magnetooptic upper claddings on semiconductor (silicon or III-V) waveguides. The form birefringence in a waveguide format prevents the required mode conversion from being achieved in a single step, but a quasi-phase-matched approach can be employed with successive half-beat-lengths of magnetooptic and non- magnetooptic waveguide sections. A brief review of initial demonstrations of QPM Faraday rotation in waveguides is provided.

Initial results and characterization of a lift-off process to obtain garnet segments on a semiconductor wafer are presented. Polycrystalline YIG was obtained after anneal at 800 °C reproducibly in fabricated segments of (sub)micron-scale horizontal dimensions and tens of nanometer thickness on silicon-on-insulator. It was found that an initial 5 nm MgO layer can improve adhesion of the garnet film. Deposition and anneal of YIG was also undertaken on GaAs. It was found that an initial 5 nm MgO layer was essential to prevent the garnet precursor reacting with the GaAs under annealing. The fabricated segments appear well defined after anneal at 700 °C, but there is roughening of the GaAs when the anneal temperature is increased to 800 °C. As the EBSD results indicate only partial crystallization at 700 °C, further process development is required in order to optimize the temperature and/or inhibit GaAs surface roughening under annealing.

It should be noted that the lift-off process developed here can include features not available by other fabrication methods, and be applied to other magnetooptic applications. For example, patterned magnetic garnet thin films may find applications in the field of spintronics as a technological solution to support spin currents and spin waves [25]. The study reported here used rectangular mask openings, but there is no reason why other shapes could not be employed. For example, the segment edges could be tapered to avoid a discontinuity in the index mismatch, and as the deposition thickness is dependent on the mask opening, the taper would automatically be incorporated into the thickness too. This deposition technique could be employed to avoid the additional optical loss that is obtained with the alternative technique of direct or adhesive bonding resulting from the garnet die edges. The lift-off fabrication process may also prove to be a technique where two-dimensional magnetophotonic structures [26] could be realized.

The QPM Faraday rotation uses polarization modes in a single contiguous waveguide in contrast to the Mach–Zehnder interferometer or ring resonator required to utilize the alternative approach based on nonreciprocal phase shifts. The principal advantage of a single contiguous waveguide is that it avoids waveguide couplers and hence uses less real estate on the chip. It is therefore particularly suited to dense optoelectronic integration formats, such as in device arrays.

The analysis and design of waveguides for QPM Faraday rotation is based on the determination of the Stokes parameters for the waveguide modes. It is shown that in an evanescent wave interaction, the need for a seed layer in the deposition of some substituted garnets can be a significant penalty on the degree of interaction.

We have based most of our analysis around a SOI waveguide of dimension 500 nm $\times$ 700 nm. This is somewhat larger than the waveguides based on the more common 220 nm (CMOS standard) silicon layer thickness. The larger waveguide dimensions provide a greater tolerance on waveguide dimensions, and the etched fabrication of asymmetric waveguides for reciprocal polarization mode conversion is more straightforward. However, it is apparent that the modal overlaps of a magnetooptic claddings results in small degree of interaction, leading to exceptionally long overall device lengths. Note that similar modal overlap requirements also apply to the nonreciprocal phase shift approach. It may be possible to incorporate long device lengths on a manageable chip size by adding waveguide bends to form a serpentine structure (similar to Ref. [6]). However, optical losses will also set a practical limit to overall device lengths. Therefore, it is anticipated that the optical mode overlap with the magnetooptic cladding must be significantly improved, while still utilizing garnet films with large Faraday rotations. As an example, a 220 nm $\times$ 300 nm SOI waveguide with alternating 100 nm of Ce:YIG and SiO_2 claddings could achieve the

required nonreciprocal polarization mode conversion in a length of 3.02 mm. Similar modal engineering strategies could be pursued for GaAs waveguides by deep dry etch into the lower cladding, and undercut etching or (partial) oxidation of the AlGaAs lower cladding.

Overall, we have demonstrated the feasibility of integrated magnetooptic technology based on silicon or III-V waveguide structures with a sputtered and annealed magnetooptic garnet as an upper cladding formed using lift-off lithography. The incorporation of a thin MgO layer proves to be useful for the adhesion of thin films, and in protecting the III-V wafer surface.

Acknowledgment

The authors acknowledge the valuable support of sample fabrication by the technical staff of the James Watt Nanofabrication Centre. The authors also thank the Minnesota Nanofabrication Center and the Characterization Facility, both of which work under partial support from the NSF National Nanotechnology Infrastructure Network (NNIN). Useful discussions with Dr. Marc Sorel (Glasgow) and Prof. Caroline Ross (MIT) are acknowledged by the authors.

References

[1] D. C. Hutchings, "Prospects for the implementation of magneto-optic elements in optoelectronic integrated circuits: A personal perspective (invited)," *J. Phys. D, Appl. Phys.*, vol. 36, no. 18, pp. 2222–2229, Sep. 2003.
[2] H. Yokoi, T. Mizumoto, and H. Iwasaki, "Nonreciprocal TE-TM mode converter with semiconductor guiding layer," *Electron. Lett.*, vol. 38, no. 25, pp. 1670–1672, Dec. 2002.
[3] Y. Shoji, T. Mizumoto, H. Yokoi, L.-W. Hsieh, and J. R. M. Osgood, "Magneto-optical isolator with silicon waveguides fabricated by direct bonding," *Appl. Phys. Lett.*, vol. 92, no. , pp. 071117-1–071117-3, Feb. 2008.
[4] Y. Shoji, M. Ito, Y. Shirato, and T. Mizumoto, "MZI optical isolator with si-wire waveguides by surface-activated direct bonding," *Opt. Exp.*, vol. 20, no. 16, pp. 18 440–18 448, Jul. 2012.
[5] S. Ghosh, S. Keyvavinia, W. V. Roy, T. Mizumoto, G. Roelkens, and R. Baets, "Ce:YIG/silicon-on-insulator waveguide optical isolator realized by adhesive bonding," *Opt. Exp.*, vol. 20, no. 2, pp. 1839–1848, Jan. 2012.
[6] S. Ghosh, S. Keyvavinia, Y. Shirato, T. Mizumoto, G. Roelkens, and R. Baets, "Optical isolator for TE polarized light realized by adhesive bonding of Ce:YIG on silicon-on-insulator waveguide circuits," *IEEE Photon. J.*, vol. 5, no. 3, p. 6601108, Jun. 2013.
[7] L. Bi, J. Hu, P. Jiang, D. H. Kim, G. F. Dionne, L. C. Kimerling, and C. A. Ross, "On-chip optical isolation in monolithically integrated non-reciprocal resonators," *Nat. Photon.*, vol. 5, no. 12, pp. 758–762, Dec. 2011.
[8] V. P. Tzolov and M. Fontaine, "A passive polarization converter free of longitudinally-periodic structure," *Opt. Commun.*, vol. 127, no. 1–3, pp. 7–13, Jun. 1996.
[9] J. Z. Huang, R. Scarrmozzino, G. Nagy, M. J. Steel, and R. M. Osgood, Jr., "Realization of a compact and single-mode optical passive polarization converter," *IEEE Photon. Technol. Lett.*, vol. 12, no. 3, pp. 317–319, Mar. 2000.
[10] B. M. Holmes and D. C. Hutchings, "Realisation of novel low-loss monolithically integrated waveguide mode converters," *IEEE Photonics Technol. Lett.*, vol. 18, no. 1, pp. 43–45, Jan. 2006.
[11] L. M. Augustin, J. J. G. M. van der Tol, E. J. Geluk, and M. K. Smit, "Short polarization converter optimized for active-passive integration in InGaAsP–InP," *IEEE Photon. Technol. Lett.*, vol. 19, no. 20, pp. 1673–1675, Oct. 2007.
[12] B. M. Holmes, M. A. Naeem, D. C. Hutchings, J. H. Marsh, and A. E. Kelly, "A semiconductor laser with monolithically integrated dynamic polarization control," *Opt. Exp.*, vol. 20, no. 18, pp. 20 545–20 550, Aug. 2012.
[13] D. C. Hutchings and B. M. Holmes, "A waveguide polarisation toolset design based on mode-beating," *IEEE Photon. J.*, vol. 3, no. 3, pp. 450–461, Jun. 2011.
[14] J. A. Armstrong, N. Bloembergen, J. Ducuing, and P. S. Pershan, "Interactions between light waves in a nonlinear dielectric," *Phys. Rev.*, vol. 127, no. 6, pp. 1918–1939, Sep. 1962.
[15] D. C. Hutchings and T. C. Kleckner, "Quasi-phase-matching in semiconductor waveguides using intermixing: Optimisation considerations," *J. Opt. Soc. Amer. B, Opt. Phys.*, vol. 19, no. 4, pp. 890–894, Apr. 2002.
[16] K. Zeaiter, D. C. Hutchings, R. Gwilliam, K. Moutzouris, S. V. Rao, and M. Ebrahimzadeh, "Quasi-phase matched second harmonic generation in GaAs/AlAs superlattice waveguide using ion-implantation induced intermixing," *Optics Lett.*, vol. 28, no. 11, pp. 911–913, Jun. 2003.
[17] S. J. Wagner, B. M. Holmes, U. Younis, I. Sigal, A. S. Helmy, J. S. Aitchison, and D. C. Hutchings, "Difference frequency generation by quasi-phase matching in periodically intermixed semiconductor superlattice waveguides," *IEEE J. Quantum Electron.*, vol. 47, no. 6, pp. 834–840, Jun. 2011.
[18] P. K. Tien, R. J. Martin, R. Wolfe, R. C. L. Craw, and S. L. Blank, "Switching and modulation of light in magneto-optic waveguides of garnet films," *Appl. Phys. Lett.*, vol. 21, no. 8, pp. 394–396, Oct. 1972.
[19] R. Wolfe, J. Hegarty, J. J. F. Dillon, L. C. Luther, G. K. Celler, and L. E. Trimble, "Magneto-optic waveguide isolators based on laser annealed (Bi, Ga) YIG films," *IEEE Trans. Magn.*, vol. MAG-21, no. 5, pp. 1647–1650, Sep. 1985.
[20] K. Ando, T. Okoshi, and N. Koshizuka, "Waveguide magneto-optic isolator fabricated by laser annealing," *Appl. Phys. Lett.*, vol. 53, no. 1, pp. 4–6, Jul. 1988.
[21] B. M. Holmes and D. C. Hutchings, "Demonstration of quasi-phase-matched non-reciprocal polarisation rotation in III–V semiconductor waveguides incorporating magneto-optic upper claddings," *Appl. Phys. Lett.*, vol. 88, no. 6, p. 061116, Feb. 2006.

[22] S.-Y. Sung, A. Sharma, A. Block, K. Keuhn, and B. J. H. Stadler, "Magneto-optical garnet waveguides on semiconductor platforms: Magnetics, mechanics and photonics," *J. Appl. Phys.*, vol. 109, no. 7, p. 07B738, Apr. 2011.
[23] A. B. Fallahkhair, K. S. Li, and T. E. Murphy, "Vector finite difference modesolver for anisotropic dielectric waveguides," *J. Lightwave Technol.*, vol. 26, no. 11, pp. 1423–1431, Jun. 2008.
[24] T. Körner, A. Heinrich, M. Weckerle, P. Roocks, and B. Stritzker, "Integration of magneto-optical active bismuth iron garnet on nongarnet substrates," *J. Appl. Phys.*, vol. 103, no. 7, pp. 07B337-1–07B337-3, Apr. 2008.
[25] Y. Kajiwara, K. Harii, S. Takahashi, J. Ohe, K. Uchida, M. Mizuguchi, H. Umezawa, H. Kawai, K. Ando, K. Takanashi, S. Maekawa, and E. Saitoh, "Transmission of electrical signals by spin-wave interconversion in a magnetic insulator," *Nature*, vol. 464, no. 7286, pp. 262–267, Mar. 2010.
[26] M. Vanwolleghem, X. Checoury, W. Migaj, B. Gralak, L. Magdenko, K. Postava, B. Dagens, P. Beauvillain, and J.-M. Lourtioz, "Unidirectional band gaps in uniformly magnetized two-dimensional magnetophotonic crystals," *Phys. Rev. B, Condens. Matter*, vol. 80, no. 12, pp. 121102-1–121102-4, Sep. 2009.